HHS Public Access

Author manuscript

Mol Genet Metab. Author manuscript; available in PMC 2019 July 13.

Published in final edited form as:

Mol Genet Metab. 2018 September ; 125(1-2): 144–152. doi:10.1016/j.ymgme.2018.06.012.

Tissue acylcarnitine status in a mouse model of mitochondrial β-oxidation deficiency during metabolic decompensation due to influenza virus infection

Tatiana N. Tarasenko[1], **Kristina Cusmano-Ozog**[2], and **Peter J. McGuire**[1]

[1]Metabolism, Infection and Immunity Section, National Human Genome Research Institute, National Institutes of Health, Bethesda, MD;

[2]Rare Disease Institute, Children's National Medical Center, Washington, DC.

Abstract

Despite judicious monitoring and care, patients with fatty acid oxidation disorders may experience metabolic decompensation due to infection which may result in rhabdomyolysis, cardiomyopathy, hypoglycemia and liver dysfunction and failure. Since clinical studies on metabolic decompensation are dangerous, we employed a preclinical model of metabolic decompensation due to infection. By infecting mice with mouse adapted influenza and using a pair-feeding strategy in a mouse model of long-chain fatty acid oxidation (*Acadvl*$^{-/-}$), our goals were to isolate the effects of infection on tissue acylcarnitines and determine how they relate to their plasma counterparts. Applying statistical data reduction techniques (Partial Least Squares-Discriminant Analysis, PLS-DA), we were able to identify critical acylcarnitines that were driving differentiation of our experimental groups for all the tissues studied. While plasma displayed increases in metabolites directly related to mouse VLCAD deficiency (e.g. C16 and C18), organs like the heart, muscle and liver also showed involvement of alternative pathways (e.g. medium chain FAO and ketogenesis), suggesting adaptive measures. Matched correlation analyses showed strong correlations ($r > 0.7$) between plasma and tissue levels for a small number of metabolites. Overall, our results demonstrate that infection as a stress produces perturbations in metabolism in *Acadvl*$^{-/-}$ that differ greatly from WT infected and *Acadvl*$^{-/-}$ pair-fed controls. This model system will be useful for studying the effects of infection on tissue metabolism as well as evaluating interventions aimed at modulating the effects of metabolic decompensation.

Keywords

fatty acid oxidation; very long-chain acyl CoA dehydrogenase deficiency; infection; influenza; acylcarnitines; liver; heart; muscle; plasma; biochemical genetics; metabolic decompensation

Corresponding author: Peter J. McGuire MS, MD, Metabolism, Infection and Immunity Section, National Human Genome Research Institute, 10 Center Drive, Room 7N260A, Bethesda, MD 20892, Phone: 301-451-7716, peter.mcguire@nih.gov.

Disclosure Statement

T.N.T., K.C.O. and P.J.M. have no conflicts of interest to declare.

1. Introduction

Fatty acid oxidation (FAO), otherwise known as β-oxidation, is a process by which fatty acids are catabolized to yield energy. Fatty acids are high in caloric content (≈9 kcal/g) and serve as a glucose sparing mechanism during fasting and times of stress [1]. Long-chain fatty acids are transported across the mitochondrial membrane by the carnitine shuttle, while medium- and short-chain fatty acids readily cross the mitochondrial membrane. Once in the matrix, the fatty acids are acted upon by a series of enzymes (e.g. dehydrogenases, hydratases and thiolases) in chain-length specific manner. For every turn of the β-oxidation spiral 2 carbons are cleaved, yielding acetyl CoA which then enters the tricarboxylic acid (TCA) cycle. Furthermore, NADH and $FADH_2$ are also produced and provide reducing equivalents for the respiratory chain via the electron transport flavoprotein [2].

Mitochondrial fatty acid oxidation disorders (FAOD) are a heterogeneous group of inborn errors of metabolism (IEM). These autosomal recessive defects in the transport or β-oxidation of fatty acids are increasingly diagnosed through state mandated newborn screening. Age of onset may be varied, ranging from neonatal onset to adult presentations. Due to the ubiquitous nature of FAO, clinical manifestations of FAOD are multisystemic and may include severe hepatopathy, cardiomyopathy, skeletal myopathy, and even encephalopathy, the pathogenesis of which is poorly understood [3].

Very long-chain acyl coA dehydrogenase deficiency (VLCADD, OMIM 609575) is the most common disorder of long-chain fatty acid oxidation with an incidence of 1:50,000 – 100:000 [4, 5]. The clinical phenotype may include exercise induced rhabdomyolysis, cardiomyopathy, and hypoketotic hypoglycemia (liver) with varying age of presentation [2]. Elevations in C14-C18 acylcarnitines may be found in plasma. The VLCAD deficient mouse (*Acadvl*$^{-/-}$) is viable and prone to stress-induced hypoglycemia, skeletal myopathy and intolerance to cold, fasting and exercise [6, 7]. In *Acadvl*$^{-/-}$, plasma acylcarnitines differ from humans, exhibiting a more limited spectrum accumulating metabolites (i.e. C16–C18), due to overlapping long-chain acyl coA dehydrogenase (LCAD) activity [8]. Despite these pathophysiologic differences, the VLCAD-deficient mouse manifests with a stress-induced phenotype similar to humans [7, 9], raising new possibilities for characterizing the effect of physiological stressors, such as infection, at the tissue level. The purpose of this study was to define the tissue-specific perturbations in a mouse model of FAO (i.e. VLCAD deficiency) due to a respiratory viral infection, a common precipitant of metabolic decompensation. To control for energy intake and isolate the effects of infection, WT and *Acadvl*$^{-/-}$ mice were pair-fed in the presence or absence of mouse adapted influenza A [10]. Following infection for 5 days, mice were sacrificed and acylcarnitine analysis was performed on the tissues commonly affected during metabolic decompensation in patients with long-chain FAO: plasma, heart, muscle and liver.

2. Materials and Methods

2.1 Infection with A/PR/8/34 (PR8)

The experiments outlined were performed on the following strains: C57Bl/6 (The Jackson Laboratory, Bar Harbor, ME), and *Acadvl*$^{-/-}$(B6;129S6-*Acadvl*^{tm1Uab}, Mutant Mouse

Regional Resource Center, Davis, CA). Littermate mice were used as controls for all experiments. Mice were housed in a pathogen-free facility, housed individually, and had access to a 24% protein mush-based feed, Nutragel (Bio-Serv, Frenchtown, NJ), and autoclaved reverse osmosis water. Temperature (22 ± 2°C) and humidity (30–70%) were maintained in a controlled environment with a 12-hour light cycle. Mouse adapted human influenza virus A/PR/8/34 (PR8) was produced as previously described [11]. Eight-week-old mice (20 – 23 grams) were exposed to 500 $TCID_{50}$ of PR8 in an aerosolizing chamber (Glas-Col, Terre Haute, IN) [10, 12, 13]. Food intake was matched by pair-feeding in all mice. Food intake according to body weight in infected mice was determined in pilot experiments and then applied to all mice with or without infection: Day 1 – 42% of body weight, Day 2 – 35% of body weight, Day 3 – 35% of body weight, Day 4 – 33% of body weight and Day 5 – 25% of body weight. On Day 5 of infection, mice were euthanized by 5% Isoflurane inhalation with cervical dislocation. All tissues were isolated, snap frozen in liquid nitrogen and stored at −80°C until use. All animal care and procedures were carried out per the criteria outlined in the “Guide for the Care and Use of Laboratory Animals” (National Academy of Sciences, National Institutes of Health (NIH publication 86–23 revised 1985)) and were authorized by the Animal Care and Use Committees of the National Human Genome Research Institute.

2.2 Biochemical parameters

Glucose testing was performed on retro-orbital collected whole blood using standard handheld glucometer (AccuCheck, Roche Diagnostics, Indianapolis, Indiana). Serum aspartate aminotransferase, alanine aminotransferase, and creatine kinase were determined via dry-slide technology (VetTest 8008, IDEXX, Columbia, MO).

2.3 Acylcarnitine analysis

Acylcarnitine profiles on tissue homogenates were performed by the Biochemical Genetics and Metabolism Laboratory, Children’s National Medical Center (Washington, DC) according to an established protocol with some modification [14]. Briefly, all tissues were collected on Day 5 of infection at euthanasia and snap frozen until further analysis. Tissues samples were homogenized in PBS and protein concentration was determined (BioRad, Hercules, CA). Samples for analysis were prepared using 30μL of Acylcarnitine Reference Standards (Cambridge Isotope Inc., Cambridge, MA), 20 μL sample, and 270 μL acetonitrile, followed by vortexing and centrifugation for 5 min. The supernatant is pulled off, dried, derivatized with 3N HCl in Butanol, dried again and reconstituted with mobile phase (acetylnitrile and dH_2O). Sample (5 μL) was injected and transported to the ion source inlet of the mass spectrometer (API 5000, AB Sciex, Framingham, MA) via an isocratic organic mobile phase eluent from HPLC pumps. Precursor Ion Scan in positive mode using precursor of 85 Da. ChemoView software was used to calculate the concentrations each acylcarnitine.

2.4 mRNA expression profiling and qRT-PCR

RNA was extracted from homogenized liver tissue using a kit (Qiagen, Germantown, MD. For RT-PCR, 1 μg of RNA was reverse transcribed to cDNA using a modified MMLV-reverse transcriptase (iScript, Bio-Rad, Hercules, CA). PCR reactions were carried using

TaqMan commercial primers (Applied Biosciences, Carlsbad, CA). qPCR results were normalized to β-actin. Reactions were cycled and quantitated with an ABI 7500 Fast Real Time PCR System (Applied Biosystems, Foster City, CA).

2.5 Data analysis and statistics

All data was normalized to tissue protein or weight when applicable. Student's T-test was applied to the comparison of two means. Due to the wide variation in metabolite ranges between different acylcarnitines in this and subsequent analyses, all results were normalized for comparison. Multivariate analyses of metabolomic data was performed by partial least squares-discriminant analysis (PLS-DA) using online tools via MetaboAnalyst 3.0 [15]. A cutoff of Variable of Importance Projection (VIP) scores was set at ≥ 1.5 or greater for identifying critical signature metabolites. Statistical significance was defined as $P < 0.05$.

3. Results

3.1 Impaired glucose homeostasis in *Acadvl*$^{-/-}$ during influenza infection

In response to infection, patients with VLCADD may develop rhabdomyolysis, hypoketotic hypoglycemia and liver dysfunction [16]. To identify which blood markers may correlate with reported patient findings during infection, *Acadvl*$^{-/-}$ and WT mice were infected with mouse adapted PR8 influenza to produce a viral pneumonia. Mice were pair-fed, with or without infection, and euthanized at 5 days with blood collection (Figure 1A). Weight loss was similar ($P > 0.05$) between all the groups, suggesting that our pair-feeding strategy was sufficient (Figure 1B). Blood and serum markers for metabolic decompensation due to a long-chain FAOD were determined. Creatine kinase (CK), a measure of muscle damage, was comparable in both mice ($P = 0.24$), indicating that the phenotype of overwhelming rhabdomyolysis was not observed (Figure 1C). Serum AST was elevated in both WT and *Acadvl*$^{-/-}$ (Figure 1D), demonstrating an equivalent hepatitis. Due to long-chain FAO deficiency, we anticipated that infected *Acadvl*$^{-/-}$ mice would display a greater decline in blood glucose. Confirming our prediction, *Acadvl*$^{-/-}$ mice presented with a 24 μg reduction in blood glucose when compared to WT (Figure 1E). In brief, these data establish a forme fruste metabolic decompensation due to infection in *Acadvl*$^{-/-}$, involving glucose homeostasis. Due to the intimate relationship between glucose homeostasis and FAO, our model may be useful for studying tissue-specific adaptations in metabolism by profiling acylcarnitines.

3.2 Elevated plasma C16 and C18 metabolites in *Acadvl*$^{-/-}$ during influenza infection

Based on our observation of impaired glucose homeostasis during infection and our published studies on FAO and influenza infection [10], we hypothesized that *Acadvl*$^{-/-}$ mice would show disease specific perturbations in plasma acylcarnitine profiles during infection. Since univariate analysis can oftentimes overlook complex relationships, we employed Partial Least Squares-Discriminant Analysis (PLS-DA) to identify patterns in our dataset [17]. For plasma, we were able to obtain good separation amongst the groups via PLS-DA, with component 1 explaining 81.2% of the variation ($P < 0.001$, Figure 2A and 2B). Variable Importance in Projection (VIP) scores help identify features that allow group discrimination, providing a tissue signature. In plasma, VIP scores (≥ 1.5) identified 6 metabolites that were

critical for differentiating the various experimental groups (Figure 2C). These metabolites were primarily C16 and C18 acylcarnitines. Metabolite trends showed 4 out of 5 of these long-chain metabolites increased in infected *Acadvl*$^{-/-}$ mice, while all decreased in WT. In summary, for the top metabolites identified by VIP analysis, plasma acylcarnitine profiles display elevations in acylcarnitine species consistent with previous reports on mouse VLCAD deficiency.

3.3 *Acadvl*$^{-/-}$ heart displays involvement of alternative metabolic pathways

After birth, the heart relies on FAO for energy production, and consequently, energy deficiency contributes to metabolic cardiomyopathy [18]. In *Acadvl*$^{-/-}$ mice, pathologic findings in the heart include microvesicular steatosis, mitochondrial proliferation, and polymorphic ventricular tachycardia, in the absence of metabolic stress [9]. As the heart resides in proximity to the site of primary infection in our model, we hypothesized that acylcarnitine perturbations would manifest during infection. Via PLS-DA, good separation was achieved amongst the groups; component 1 explained 51.6% of the variation ($P < 0.001$, Figure 3A and 3B). VIP scores (≥ 1.5) provided 6 acylcarnitines, C6, C7, C12, C14, C18 and C18:1, that allowed for group discrimination (Figure 3C). In general, the relative concentrations of these 6 acylcarnitines were lower in *Acadvl*$^{-/-}$. C18 metabolites tended to decrease during infection in both groups, while C7, C12 and C14 tended to increase. Overall, our results suggest that influenza infection does lead to perturbations in heart acylcarnitine status, with *Acadvl*$^{-/-}$ mice displaying some differences in key acylcarnitines not directly related to their primary enzymatic deficiency.

3.4 *Acadvl*$^{-/-}$ muscle displays markers of medium chain FAO and ketosis

Following exercise, long-chain acylcarnitines increased 2.5x over baseline and 6x over unstressed WT mice in gastrocnemius muscle from *Acadvl*$^{-/-}$ mice [7]. Given the stress associated with infection, we hypothesized that muscle acylcarnitines would be elevated. Since gastrocnemius is a mixed fiber type muscle, we targeted a muscle composed of slow twitch fibers, i.e. soleus muscle, due to its preference for fatty acids as a fuel source [19]. Separation was obtained amongst the groups using PLS-DA, with component 1 explaining 66.5% of the variation ($P < 0.002$, Figure 4A and 4B). VIP scores (≥ 1.5) marked 3 metabolites, C4-OH, C6, and C10:1-OH, as key factors driving group discrimination (Figure 4C). Unlike WT, the relative concentrations of C6 and C10:1-OH, were lower. However, C6 and C10:1-OH trended in opposite directions in *Acadvl*$^{-/-}$ (upward) versus WT (downward) during infection. Interestingly, C4-OH (3-hydroxybutyrylcarnitine) was the top metabolite in our VIP analysis, elevated in *Acadvl*$^{-/-}$ pair-fed animals and increasing with infection, while WT displayed the opposite trend. This finding in *Acadvl*$^{-/-}$ suggests that ketosis may be taking place in muscle tissue.

3.5 *Acadvl*$^{-/-}$ liver displays markers of medium chain FAO and ketogenesis

Unlike the heart and muscle, the liver is a metabolic and immunologic organ, containing resident immune cells. As such, viremia can activate innate immune cells in the liver leading to the secretion of soluble mediators which modulate hepatic metabolism [20]. In our infection system, we were able to detect the presence of influenza in the liver by qPCR (Figure S1A) consistent with viremia. The liver responded to the viremia by increased

mRNA expression of the acute phase response (Figure S1B) and antiviral signaling components (Figure S1C). Analysis of liver acylcarnitines by PLS-DA allowed us to reasonably separate the four experimental conditions (Figure 5A). Component 1 accounted for 35.3% of the variation ($P < 0.001$, Figure 5B). C5DC, C6DC, C8, C12-OH, and C14:2 acylcarnitines were the main drivers (VIP scores ≈ 1.5 or greater) of group discrimination (Figure 5C). Interestingly, C6DC (ketogenesis) and C8 (medium chain FAO) were the top metabolites in our VIP analysis. These top metabolites were elevated during pair feeding and increased with infection in *Acadvl*$^{-/-}$, while WT showed a similar trajectory during infection, albeit at attenuated levels. Although not a defining metabolite in PLS-DA differentiation, C4-OH also increased during infection (data not shown) consistent with ketosis. Similar to the heart and muscle, the liver appears to engage alternative pathways to compensate for long-chain FAO deficiency via medium chain FAO and ketogenesis.

3.6 Plasma and tissue acylcarnitines correlations show a very limited relationship

To address the relationship between the metabolites with VIP scores ≥1.5 in each tissue with their respective plasma levels, we performed a matched correlation analysis (Figure 6). In the heart (Figure 6A), strong positive correlations ($r > 0.7$) were seen for long-chains C14 in pair-fed WT, and C6 and C12 in infected WT. *Acadvl*$^{-/-}$ failed to display any strong positive correlations. Muscle tissue showed strong positive correlations ($r > 0.7$) for C4-OH in both WT and *Acadvl*$^{-/-}$ during infection (Figure 6B), the levels of which trended in opposite directions (Figure 4C). *Acadvl*$^{-/-}$ liver C6DC demonstrated a strong correlation ($r > 0.7$) with plasma during infection (Fig 6C), which, unlike WT, tended to increase (Figure 5C). While the top acylcarnitines identified by VIP scores did not reflect tissue status, our matched correlation analysis is consistent with the liver as a source of ketones to fuel muscle.

4. Discussion

Studying metabolic decompensation as a naturally occurring experiment in patients with FAOD presents multiple challenges to the investigator including the effects of multiple variables inherent in clinical care, as well as the danger involved to patients. Preclinical models of metabolic decompensation due to infection, as presented herein, can serve as a gateway to understanding pathophysiology in a controlled manner as well as a platform for evaluating targeted therapeutics. Our findings demonstrate that influenza infection differentially affects tissues in murine VLCAD deficiency producing tissue-specific acylcarnitine perturbations.

Although no formal studies exist on the precipitants of metabolic decompensation in patients with FAOD, it is generally reported that infection is a major cause [21, 22]. Nonetheless, it is necessary to reframe our understanding of metabolic decompensation due to infection. While the medical literature on metabolic decompensation in FAOD oftentimes groups infection with other catabolic stresses, we disagree with this rather broad inclusion. While catabolism is certainly a component of infection, there are other aspects of the pathophysiology of infection that make it unique. A prime example involves the conservation of fuels and energy. Unlike other catabolic states, metabolic fuels and energy

are not conserved during infection. Two catabolic states, starvation and infection highlight further these differences. During starvation, basal metabolic rates (BMR) are downregulated and nitrogen is reabsorbed in the kidney while infection leads to opposite effects [1, 10, 23]. These aspects of infection place the organism at risk for metabolic imbalances, further exacerbating catabolism [24, 25].

Our pair feeding approach helps to further delineate the differences in the catabolic stresses employed (i.e. food restriction versus food restriction + infection) in our model. Infected animals experience a drop in blood glucose due a downregulation (WT) [10] or the loss (*Acadvl*$^{-/-}$) of glucose sparing FAO. As noted above, impaired reabsorption of gluconeogenic amino acids via the kidney is also a compounding factor. The importance of FAO in glucose homeostasis during influenza infection has also been indicated in another model of FAOD. Sinde et al. proposed that *Acadl*$^{-/-}$ mice infected with pandemic influenza displayed a greater reliance on glucose for energy, and as a result experienced greater mortality due to bioenergetic starvation [26]. As evidence for dependence upon glycolysis, elevated lactate was found in *Acadl*$^{-/-}$. However, unlike our studies with *Acadvl*$^{-/-}$, a depression in blood glucose was not seen. This disparity may be readily explained by differences in influenza strain, pathogenicity, feeding strategy, and type of FAO deficiency. More importantly, both studies do succeed in demonstrating the importance of FAO for glucose homeostasis during respiratory viral infection and has implications regarding treatment strategies during metabolic decompensation due to infection.

Previous models of metabolic decompensation in VLCAD deficiency have utilized a range of stresses including changes in dietary composition, cold, fasting and exercise [6–9, 27–30]. Some of the seminal studies on blood and tissue acylcarnitines under stress conditions were published by Spierkerkotter et al. [6, 7]. VLCAD deficient mice were subjected to exercise, cold, and fasting with quantitation of blood and tissue acylcarnitines. VLCAD deficient mice had characteristic elevations in C16-C18 acylcarnitines. However, similar to most studies on VLCAD mice, the data were focused on disease-centric metabolites such as carnitine, acetyl carnitine and long-chain acylcarnitines. Rather than specifically looking at disease-specific metabolites, we chose to identify tissue-specific metabolite signatures using PLS-DA [17]. Besides perturbations in C16-C18 acylcarnitines, we also found changes in metabolites that reflect the engagement of alternative metabolic pathways to compensate for FAO deficiency during metabolic decompensation due to infection.

Acadvl$^{-/-}$ mice can exhibit tissue-specific adaptations in FAO in response changes in dietary fat. On a diet composed of medium-chain triglycerides and absent of long-chain triglycerides, components of medium-chain FAO are upregulated [28]. This suggests that tissues may have an inherent flexibility regarding metabolic fuel choice under stressful situations. The adaptability of tissue metabolism to stress occurs via metabolic reprogramming and is termed allostasis. Tissue metabolic reprogramming in response to infection in *Acadvl*$^{-/-}$ has not been characterized to date, prompting us to explore this adaptation. Accumulations of C12 medium-chains were seen in the heart, muscle and liver of *Acadvl*$^{-/-}$ during infection, potentially reflecting increased transport and utilization of alternative substrates via residual fatty acid oxidation with LCAD, or possibly MCAD. Certainly, C6, C8, C10 acylcarnitines were also found to be increased in *Acadvl*$^{-/-}$ tissues,

further supporting an allostatic mechanism utilizing medium chain FAO [28]. The adoption of medium chain FAO makes biologic sense, given that the utility and energetic impact of medium chain fatty acids is well documented. Compared to long-chain fatty acid-treated cells, medium chain fatty acids increase mitochondrial oxidative capacity [31, 32]. The benefits of employing medium chain FAO can also be seen clinically. In patients with VLCAD deficiency, supplementation with medium chain triglycerides as an energy source can bypass the block in FAO and help avoid metabolic decompensation [33, 34].

In addition to increased medium chain acylcarnitines, markers of ketogenesis could be seen in muscle and liver. A means of increasing ketones involves the consumption of medium-chain triglycerides, and by extension the activation of medium-chain FAO [35]. Unlike long-chain fatty acids, medium-chain fatty acids do not need the carnitine shuttle to access the inner mitochondrial membrane for β-oxidation. As a result, medium-chain fatty acids are rapidly broken down readily yielding substrates for ketogenesis. Given our data on medium-chain acylcarnitines, we suspect that endogenous medium-chain FAO in the liver may be upregulated in *Acadvl*$^{-/-}$ during infection enabling ketogenesis to feed muscle. C4-OH muscle/plasma correlations suggest this. Furthermore, C4-OH was significantly higher in *Acadvl*$^{-/-}$ versus WT muscle during pair-feeding and even increased during infection, while WT had an opposite response. In the livers of infected *Acadvl*$^{-/-}$ mice, C6DC was a defining metabolite by PLS-DA, and C4-OH was also increased, further supporting the liver as the source of ketones. Liver/plasma correlations support this assertion. Although this may seem contrary to our understanding of the clinical picture of long-chain FAO, the relationship between FAO and ketogenesis may be more complex. Certainly, ketonuria has been reported in patients with VLCAD deficiency whose diagnosis was confirmed by molecular testing [36]. In addition, patients with long-chain FAO on MCT therapy certainly develop urine ketones, indicating that medium-chain FAO can be leveraged as an energy source [37]. Based on these data and our results, it is reasonable to suggest that tissues affected by VLCAD deficiency may develop the aforementioned adoptive strategies in FAO to meet their energetic needs.

5. Conclusions

In conclusion, we have established a preclinical model of metabolic decompensation due to infection in a mouse model of mitochondrial β-oxidation deficiency. The *Acadvl*$^{-/-}$ model displays a stress-induced phenotype similar to humans making it useful for studying the unique physiologic aspects of infection, metabolic decompensation, and interventions aimed at abrogating these effects. During infection with mouse adapted PR8 influenza, A*cadvl*$^{-/-}$ mice display altered glucose homeostasis and tissue-specific metabolic adaptations which may involve the engagement of medium chain fatty acid oxidation and ketogenesis. These tissue-specific adaptations are not well represented in plasma acylcarnitines, indicating limited clinical utility for monitoring.

Supplementary Material

Refer to Web version on PubMed Central for supplementary material.

Acknowledgements

We would like to thank the Animal Facility of National Human Genome Research Institute.

Funding

This work was supported by the intramural research program of the National Institutes of Health (HG200381–03).

6. References

[1]. Hue L, Taegtmeyer H, The Randle cycle revisited: a new head for an old hat Am J Physiol Endocrinol Metab 297 (2009) E578–591. [PubMed: 19531645]

[2]. Spiekerkoetter U, Mayatepek E, Update on mitochondrial fatty acid oxidation disorders J Inherit Metab Dis 33 (2010) 467–468.

[3]. Wajner M, Amaral AU, Mitochondrial dysfunction in fatty acid oxidation disorders: insights from human and animal studies Biosci Rep 36 (2015) e00281. [PubMed: 26589966]

[4]. Arnold GL, Van Hove J, Freedenberg D, Strauss A, Longo N, Burton B, Garganta C, Ficicioglu C, Cederbaum S, Harding C, Boles RG, Matern D, Chakraborty P, Feigenbaum A, A Delphi clinical practice protocol for the management of very long chain acyl-CoA dehydrogenase deficiency Mol Genet Metab 96 (2009) 85–90. [PubMed: 19157942]

[5]. Spiekerkoetter U, Mitochondrial fatty acid oxidation disorders: clinical presentation of long-chain fatty acid oxidation defects before and after newborn screening J Inherit Metab Dis 33 (2010) 527–532. [PubMed: 20449660]

[6]. Spiekerkoetter U, Tokunaga C, Wendel U, Mayatepek E, Exil V, Duran M, Wijburg FA, Wanders RJA, Strauss AW, Changes in blood carnitine and acylcarnitine profiles of very long-chain acyl-CoA dehydrogenase-deficient mice subjected to stress Eur J Clin Invest 34 (2004) 191–196. [PubMed: 15025677]

[7]. Spiekerkoetter U, Tokunaga C, Wendel U, Mayatepek E, Ijlst L, Vaz FM, van Vlies N, Overmars H, Duran M, Wijburg FA, Wanders RJ, Strauss AW, Tissue carnitine homeostasis in very-long-chain acyl-CoA dehydrogenase-deficient mice Pediatr Res 57 (2005) 760–764. [PubMed: 15774826]

[8]. Cox KB, Hamm DA, Millington DS, Matern D, Vockley J, Rinaldo P, Pinkert CA, Rhead WJ, Lindsey JR, Wood PA, Gestational, pathologic and biochemical differences between very long-chain acyl-CoA dehydrogenase deficiency and long-chain acyl-CoA dehydrogenase deficiency in the mouse Hum Mol Genet 10 (2001) 2069–2077. [PubMed: 11590124]

[9]. Exil VJ, Roberts RL, Sims H, McLaughlin JE, Malkin RA, Gardner CD, Ni G, Rottman JN, Strauss AW, Very-long-chain acyl-coenzyme a dehydrogenase deficiency in mice Circ Res 93 (2003) 448–455. [PubMed: 12893739]

[10]. Tarasenko TN, Singh LN, Chatterji-Len M, Zerfas PM, Cusmano-Ozog K, McGuire PJ, Kupffer cells modulate hepatic fatty acid oxidation during infection with PR8 influenza Biochim Biophys Acta 1852 (2015) 2391–2401. [PubMed: 26319418]

[11]. Fernandez-Sesma A, Marukian S, Ebersole BJ, Kaminski D, Park MS, Yuen T, Sealfon SC, Garcia-Sastre A, Moran TM, Influenza virus evades innate and adaptive immunity via the NS1 protein J Virol 80 (2006) 6295–6304. [PubMed: 16775317]

[12]. Moltedo B, Lopez CB, Pazos M, Becker MI, Hermesh T, Moran TM, Cutting edge: stealth influenza virus replication precedes the initiation of adaptive immunity Journal of immunology 183 (2009) 3569–3573.

[13]. McGuire PJ, Tarasenko TN, Wang T, Levy E, Zerfas PM, Moran T, Lee HS, Bequette BJ, Diaz GA, Acute metabolic decompensation due to influenza in a mouse model of ornithine transcarbamylase deficiency Dis Model Mech 7 (2014) 205–213. [PubMed: 24271778]

[14]. Rinaldo P, Cowan TM, Matern D, Acylcarnitine profile analysis Genet Med 10 (2008) 151–156.

[15]. Xia J, Wishart DS, Using MetaboAnalyst 3.0 for Comprehensive Metabolomics Data Analysis Curr Protoc Bioinformatics 55 (2016) 14 10 11–14 10 91.

[16]. Pons R, Cavadini P, Baratta S, Invernizzi F, Lamantea E, Garavaglia B, Taroni F, Clinical and molecular heterogeneity in very-long-chain acyl-coenzyme A dehydrogenase deficiency Pediatr Neurol 22 (2000) 98–105. [PubMed: 10738914]

[17]. Bartel J, Krumsiek J, Theis FJ, Statistical methods for the analysis of high-throughput metabolomics data Comput Struct Biotechnol J 4 (2013) e201301009. [PubMed: 24688690]

[18]. Roe CR, Diagnostic approach to disorders of fat oxidation International Pediatrics 11 (1996) 109–113.

[19]. Zierath JR, Hawley JA, Skeletal muscle fiber type: influence on contractile and metabolic properties PLoS Biol 2 (2004) e348. [PubMed: 15486583]

[20]. Likos AM, Kelvin DJ, Cameron CM, Rowe T, Kuehnert MJ, Norris PJ, National Heart L.B.I.R.E.D.S. II, Influenza viremia and the potential for blood-borne transmission Transfusion 47 (2007) 1080–1088. [PubMed: 17524100]

[21]. Saudubray JM, Martin D, de Lonlay P, Touati G, Poggi-Travert F, Bonnet D, Jouvet P, Boutron M, Slama A, Vianey-Saban C, Bonnefont JP, Rabier D, Kamoun P, Brivet M, Recognition and management of fatty acid oxidation defects: a series of 107 patients J Inherit Metab Dis 22 (1999) 488–502. [PubMed: 10407781]

[22]. Taroni F, Uziel G, Fatty acid mitochondrial beta-oxidation and hypoglycaemia in children Curr Opin Neurol 9 (1996) 477–485. [PubMed: 9007409]

[23]. MacLeod EL, Hall KD, McGuire PJ, Computational modeling to predict nitrogen balance during acute metabolic decompensation in patients with urea cycle disorders J Inherit Metab Dis 39 (2016) 17–24. [PubMed: 26260782]

[24]. Beisel WR, Metabolic response to infection Annu Rev Med 26 (1975) 9–20. [PubMed: 1096783]

[25]. Bratovanov D, [A new method of determining and analyzing seasonality of acute infectious diseases] Zhurnal mikrobiologii, epidemiologii, i immunobiologii 47 (1970) 62–67.

[26]. Shinde A, Luo J, Bharathi SS, Shi H, Beck ME, McHugh KJ, Alcorn JF, Wang J, Goetzman ES, Increased mortality from influenza infection in long-chain acyl-CoA dehydrogenase knockout mice Biochem Biophys Res Commun 497 (2018) 700–704. [PubMed: 29458021]

[27]. Tucci S, Flogel U, Hermann S, Sturm M, Schafers M, Spiekerkoetter U, Development and pathomechanisms of cardiomyopathy in very long-chain acyl-CoA dehydrogenase deficient (VLCAD(−/−)) mice Biochim Biophys Acta 1842 (2014) 677–685. [PubMed: 24530811]

[28]. Tucci S, Herebian D, Sturm M, Seibt A, Spiekerkoetter U, Tissue-specific strategies of the very-long chain acyl-CoA dehydrogenase-deficient (VLCAD−/−) mouse to compensate a defective fatty acid beta-oxidation PloS one 7 (2012) e45429. [PubMed: 23024820]

[29]. ter Veld F, Primassin S, Hoffmann L, Mayatepek E, Spiekerkoetter U, Corresponding increase in long-chain acyl-CoA and acylcarnitine after exercise in muscle from VLCAD mice Journal of lipid research 50 (2009) 1556–1562. [PubMed: 18980943]

[30]. Tucci S, Primassin S, Spiekerkoetter U, Fasting-induced oxidative stress in very long chain acyl-CoA dehydrogenase-deficient mice Febs Journal 277 (2010) 4699–4708. [PubMed: 20883455]

[31]. Montgomery MK, Osborne B, Brown SH, Small L, Mitchell TW, Cooney GJ, Turner N, Contrasting metabolic effects of medium-versus long-chain fatty acids in skeletal muscle Journal of lipid research 54 (2013) 3322–3333. [PubMed: 24078708]

[32]. Seaton TB, Welle SL, Warenko MK, Campbell RG, Thermic effect of medium-chain and long-chain triglycerides in man Am J Clin Nutr 44 (1986) 630–634. [PubMed: 3532757]

[33]. Cox GF, Souri M, Aoyama T, Rockenmacher S, Varvogli L, Rohr F, Hashimoto T, Korson MS, Reversal of severe hypertrophic cardiomyopathy and excellent neuropsychologic outcome in very-long-chain acyl-coenzyme A dehydrogenase deficiency J Pediatr-Us 133 (1998) 247–253.

[34]. Brown-Harrison MC, Nada MA, Sprecher H, Vianey-Saban C, Farquhar J Jr., Gilladoga AC, Roe CR, Very long chain acyl-CoA dehydrogenase deficiency: successful treatment of acute cardiomyopathy Biochem Mol Med 58 (1996) 59–65. [PubMed: 8809347]

[35]. Courchesne-Loyer A, Fortier M, Tremblay-Mercier J, Chouinard-Watkins R, Roy M, Nugent S, Castellano CA, Cunnane SC, Stimulation of mild, sustained ketonemia by medium-chain triacylglycerols in healthy humans: estimated potential contribution to brain energy metabolism Nutrition 29 (2013) 635–640. [PubMed: 23274095]

[36]. Wraige E, Champion MP, Turner C, Dalton RN, Fat oxidation defect presenting with overwhelming ketonuria Arch Dis Child 87 (2002) 428–429; discussion 428–429. [PubMed: 12390922]

[37]. Olpin SE, Implications of impaired ketogenesis in fatty acid oxidation disorders Prostaglandins Leukot Essent Fatty Acids 70 (2004) 293–308. [PubMed: 14769488]

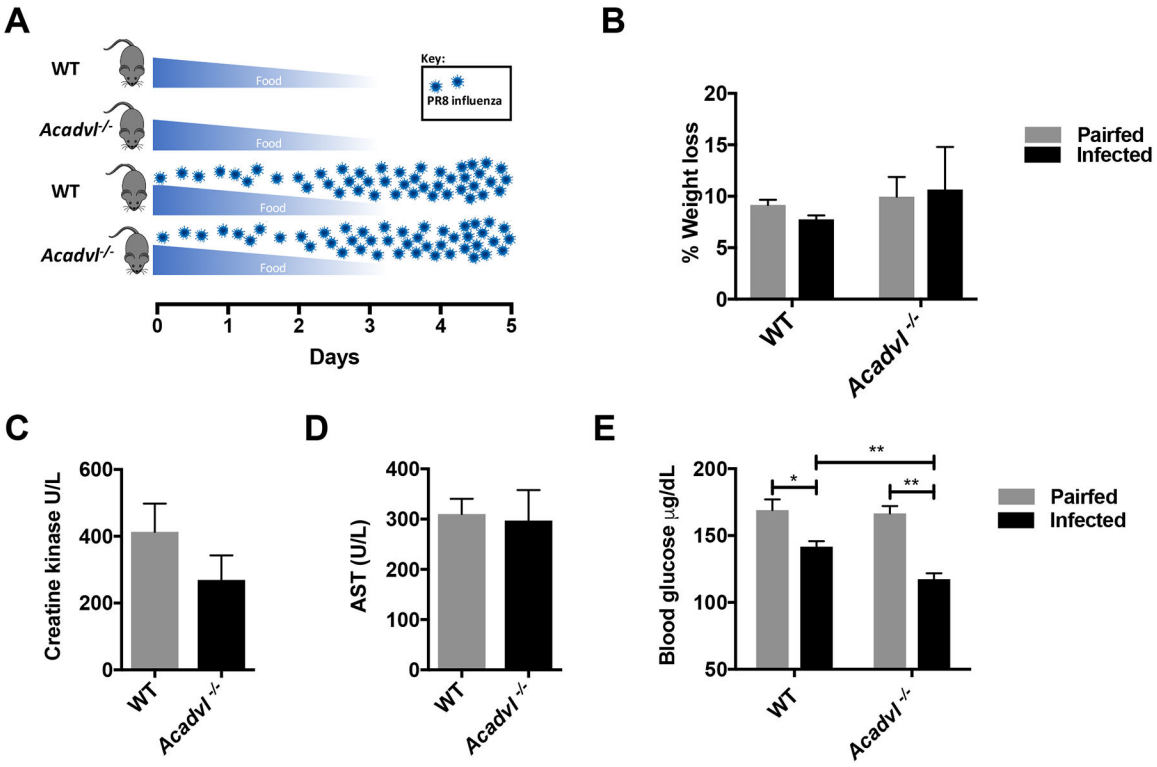

Figure 1. PR8 influenza infection in *Acadvl*$^{-/-}$ mice.

A) Experimental design. Eight-week-old mice (N = 5 / group, 20 −23 grams) were matched for food intake with or without influenza infection and euthanized at Day 5. B) Weight loss; C) Serum creatine kinase; D) Serum aspartate amino transferase (AST); E) Blood glucose. *P < 0.05, **P < 0.01.

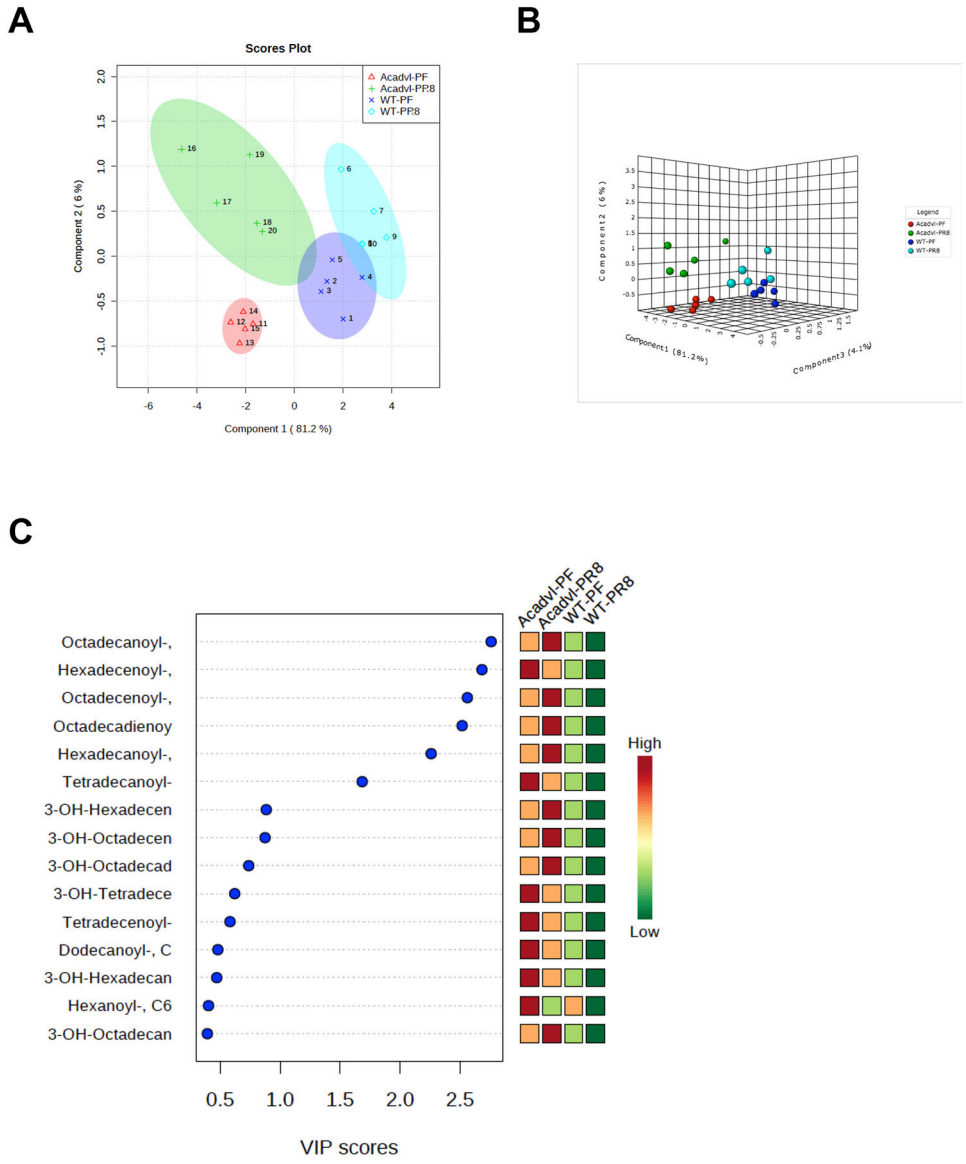

Figure 2. Plasma acylcarnitine profiles.

Mice (N = 5/group) were infected with mouse adapted influenza and euthanized on Day 5. Plasma was collected via terminal bleeding and frozen until further use. Acylcarnitine analysis was performed using LC-MS/MS. Data were normalized and partial least squares discriminant analysis (PLS-DA) was performed to determine metabolic signatures driving group separation. A) Two dimensional PLS-DA scores plot; B) Three dimensional PLS-DA scores plot; C) Variable importance in projection (VIP) scores.

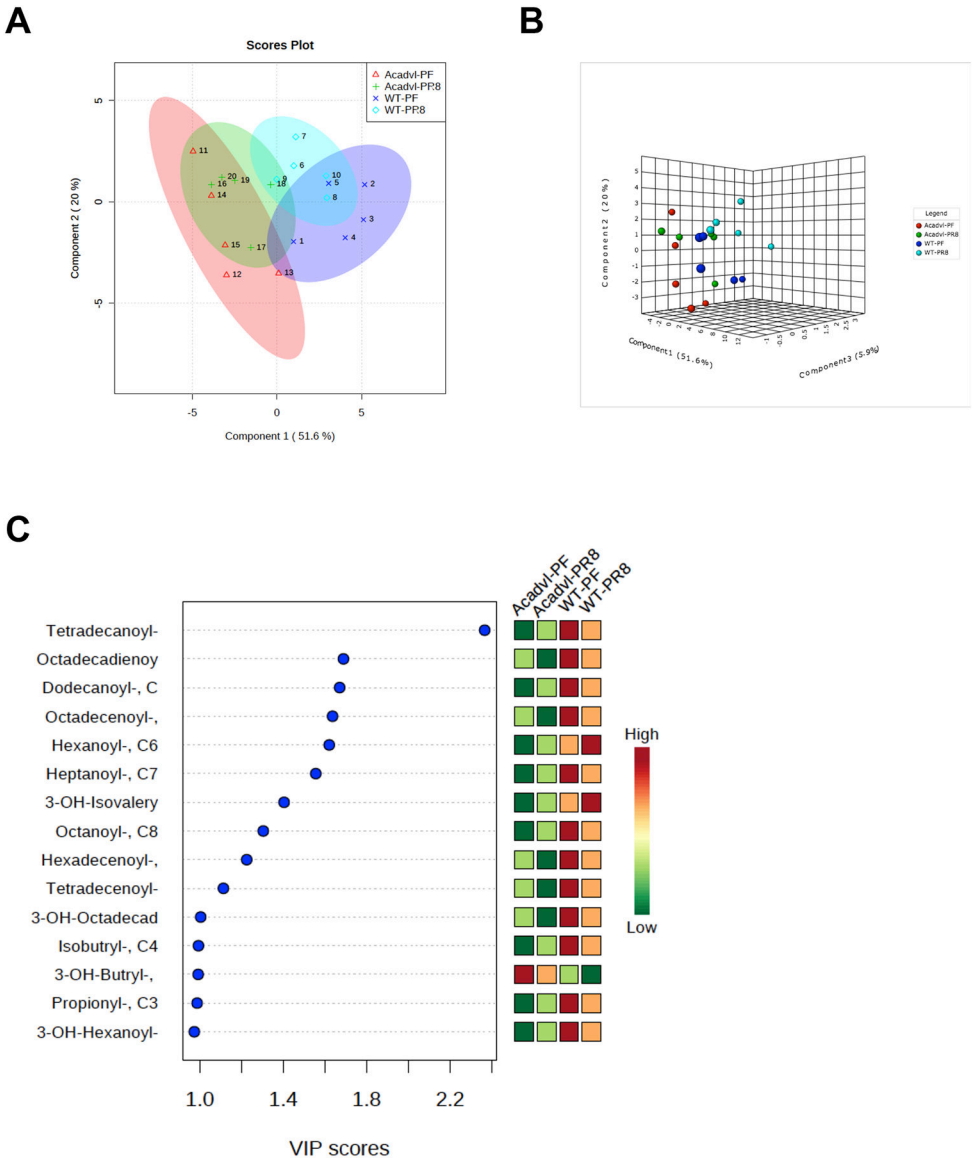

Figure 3. Heart acylcarnitine profiles.

Mice (N = 5/group) were infected with mouse adapted influenza and euthanized on Day 5. Whole hearts were collected and frozen until further use. Acylcarnitine analysis was performed using LC-MS/MS. Data were normalized and partial least squares discriminant analysis (PLS-DA) was performed to determine metabolic signatures driving group separation. A) Two dimensional PLS-DA scores plot; B) Three dimensional PLS-DA scores plot; C) Variable importance in projection (VIP) scores.

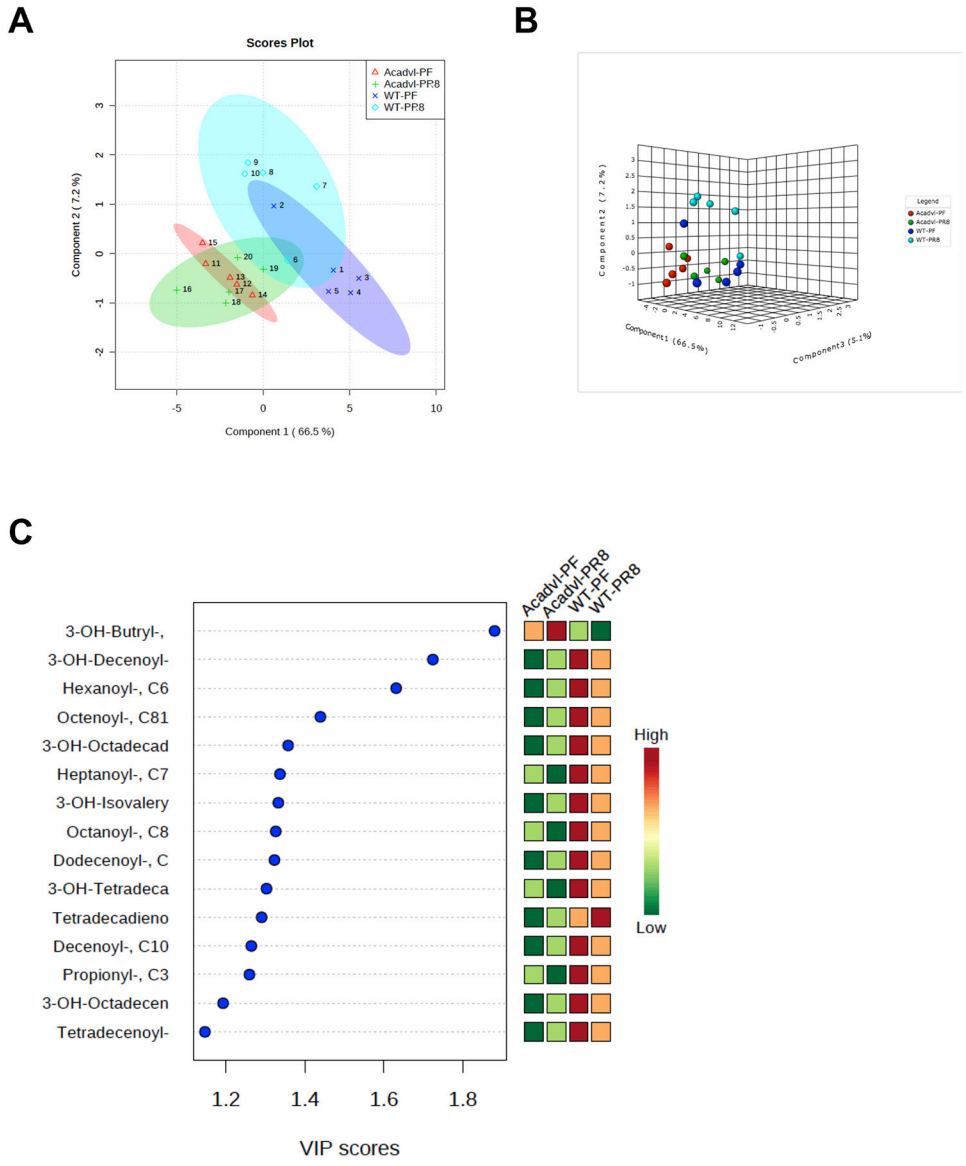

Figure 4. Muscle acylcarnitine profiles.

Mice (N = 5/group) were infected with mouse adapted influenza and euthanized on Day 5. Soleus muscles were collected and frozen until further use. Acylcarnitine analysis was performed using LC-MS/MS. Data were normalized and partial least squares discriminant analysis (PLS-DA) was performed to determine metabolic signatures driving group separation. A) Two dimensional PLS-DA scores plot; B) Three dimensional PLS-DA scores plot; C) Variable importance in projection (VIP) scores.

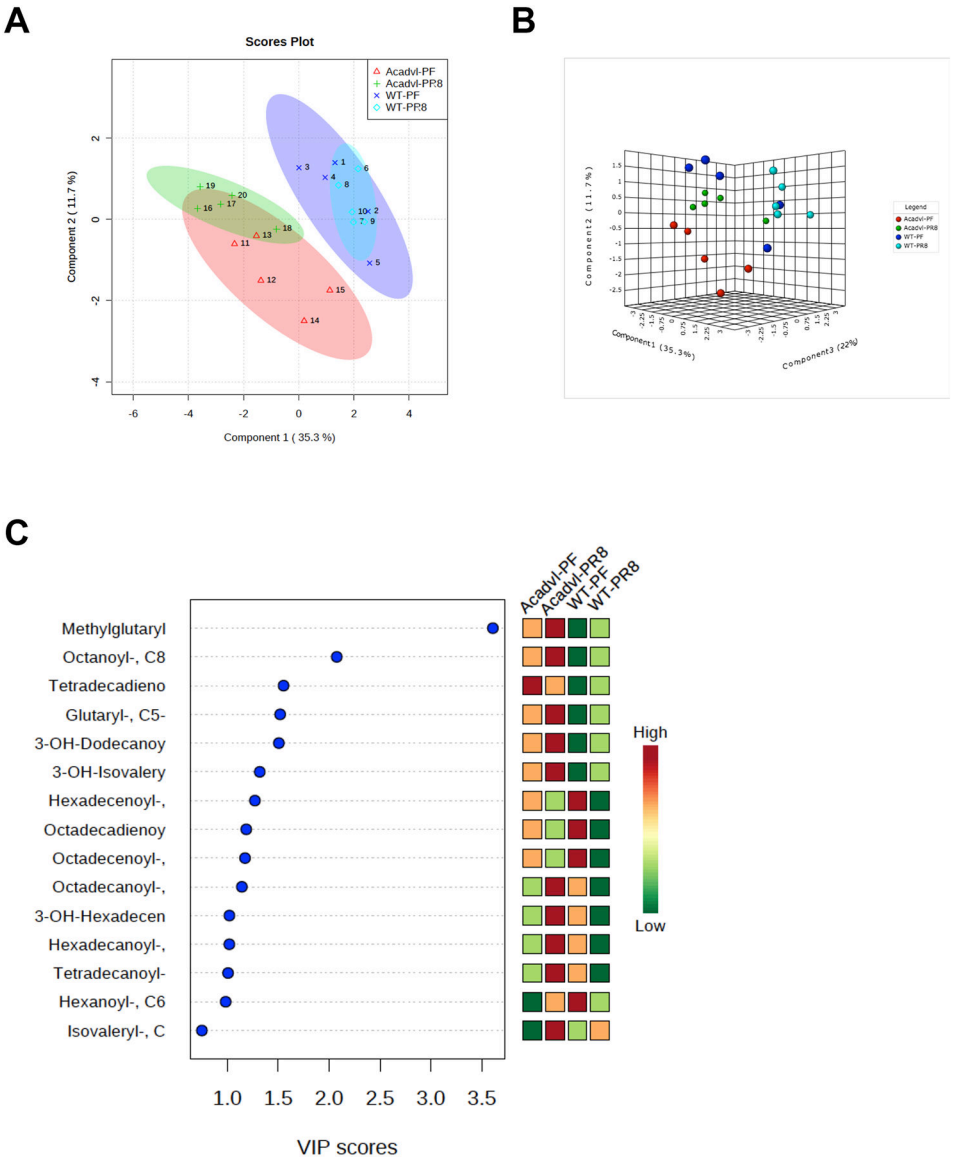

Figure 5. Liver acylcarnitine profiles.

Mice (N = 5/group) were infected with mouse adapted influenza and euthanized on Day 5. Liver tissue was collected and frozen until further use. Acylcarnitine analysis was performed using LC-MS/MS. Data were normalized and partial least squares discriminant analysis (PLS-DA) was performed to determine metabolic signatures driving group separation. A) Two dimensional PLS-DA scores plot; B) Three dimensional PLS-DA scores plot; C) Variable importance in projection (VIP) scores.

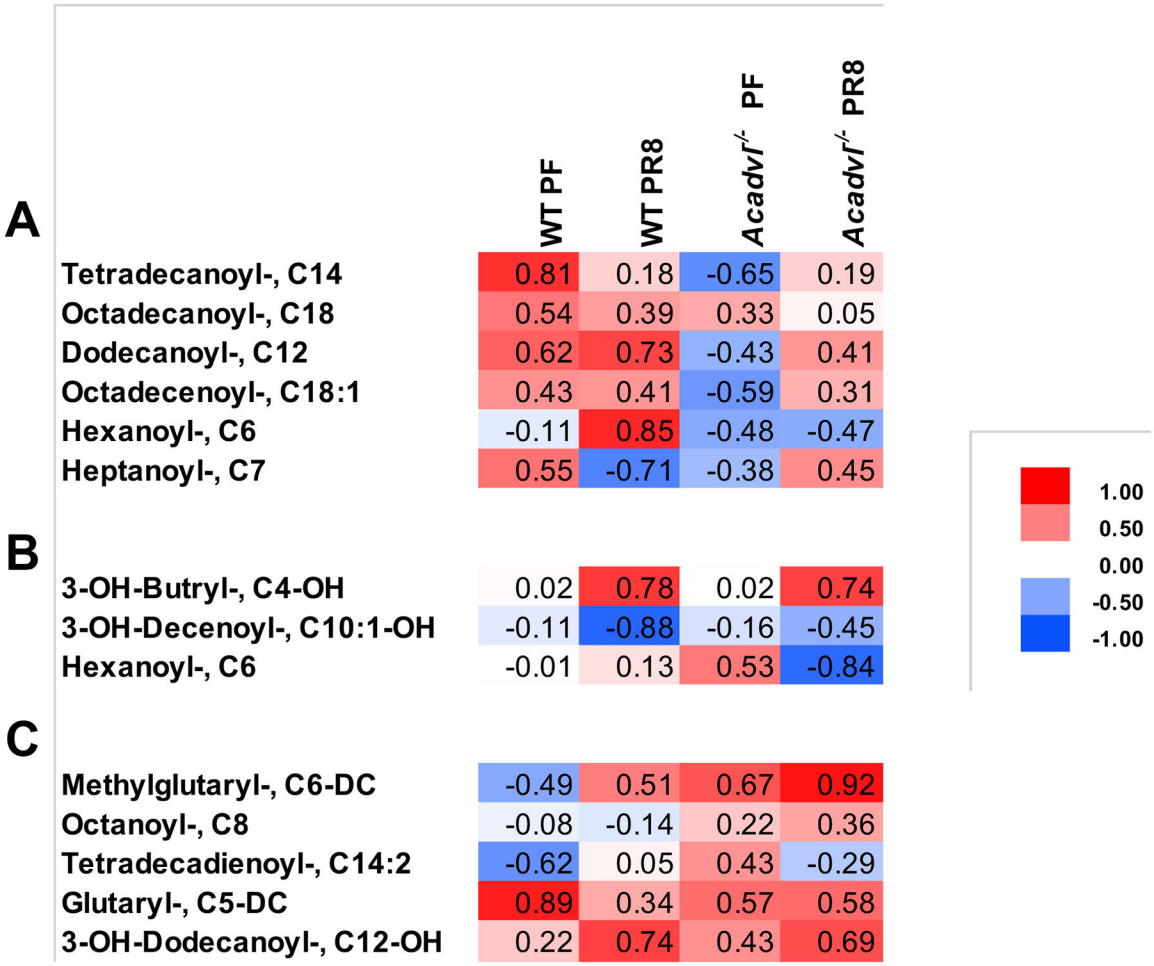

Figure 6. Plasma/tissue correlations for top 5 VIP metabolites.

Acylcarnitine values were normalized and a matched correlation analysis was performed between plasma and the following tissues: A) Heart; B) Muscle; C) Liver.